

Journal of Mechanics of Materials and Structures

THE ROCKING: A RESOURCE FOR THE SIDE STRENGTH
OF MASONRY STRUCTURES

Mario Como

Volume 14, No. 5

December 2019



THE ROCKING: A RESOURCE FOR THE SIDE STRENGTH OF MASONRY STRUCTURES

MARIO COMO

Masonry constructions activate rocking motions endeavouring to elude the action of horizontal impulse accelerations, typical of seismic actions. They can reach the dynamical collapse under acceleration impulse with intensity much higher than the one that causes the static collapse. Sudden changes of mechanisms take place during the rocking with the occurrence of impacts and consequent energy losses. Research on the topic has been generally carried out examining various schemes of structural components, as a rule considered or as a solid block or subdivided in a sequence of blocks connected by hinges. Innovative aspect of the paper, on the contrary, that collects also some results of the author, is the analysis of the influence on the rocking motion at the onset of oblique cracks that sway diagonally during the rocking of masonry walls.

1. Introduction

Masonry constructions behave under seismic actions very differently from reinforced concrete and steel structures. Masonry constructions endeavour to elude the seismic action activating a rocking motion rather than deforming with doubtful dissipating mechanisms.

Rocking is a direct consequence of the no-tension behavior of the masonry material. A masonry pier or a masonry wall, hit by a sudden horizontal impulse, moves sideways and detaches from its bases and, if does not overturn, once reached its maximum side displacement inverts its motion going back to the initial position, and so on. The pier continues to move with oscillations of reducing amplitudes and periods, until the stop of the motion.

The study of the rocking and the discovery of its importance in the seismic strength assessment of masonry buildings started with a fundamental paper of Housner [1963], in which he studied the rocking motion of a stone column resting on a rigid base. The Housner's paper showed the reasons for which tall and slender columns were able to survive severe ground shaking whereas more stable appearing reinforced concrete structures were severely damaged.

Only more recently interest in the study of rocking increased noteworthy and many contributions, involving the dynamical behavior of some simple masonry structures under various types of dynamical actions, have been given [Yim et al. 1980; Hogan 1992; Giannini and Masiani 1996; Liberatore et al. 2002; Sorrentino et al. 2006; 2008; Peña et al. 2007; Di Carlo 2014; Coccia et al. 2016], generally analysing models composed by rigid blocks.

Innovative aspect of the paper, on the contrary, that collects also some results of the author and others [Coccia et al. 2016; Di Carlo et al. 2017], is the analysis of the influence of the onset of oblique cracks swaying diagonally during the rocking of masonry piers and walls. In this context the present paper

Keywords: masonry piers and walls, rocking, cracking, acceleration pulse.

points out more clearly the differences existing between the rocking response of the solid column and that of a masonry pier or of a masonry wall, composed by two piers and one spandrel, whose piers crack diagonally during the motion.

Analysis of rocking requires the study of the impacts, that take place during the motion, to estimate the corresponding energy losses. Still more exhaustively is here studied the problem of the localization of points where impacts take place, as between piers and basement, and as between piers and spandrel.

The paper assumes, as dynamical action, the impulse of a constant horizontal acceleration A and duration t , particularly advantageous to deal with the response of structures to seismic actions via analytical approach. This loading is the dynamical extension of the common pushover statical action. Thus, if the magnitude of the acceleration impulse is higher than the limit value A_L , obtained by limit analysis, the cracked pier or the wall with openings, starts to move, overturning at base corner. By further increasing the acceleration level A_0 the pier, at a definite time t_0 , reaches a configuration at which the opposing action of the weight vanishes and dynamically fails.

The research of the dependence of the ratio A_0/A_L upon the limit duration t_0 is crucial to define the seismic strength capacity of the masonry wall. This ratio A_0/A_L represents the strength reduction factor q that has great importance in the assessment of the seismic strength of masonry constructions [Peña et al. 2007; Sorrentino et al. 2008; Di Carlo 2014; Coccia et al. 2016; Di Carlo et al. 2017; \geq 2019; Heyman 1992; Ochserdorf 2002; Como 2016].

2. Recalls of the rocking of the solid column

The discovery of the importance of studying rocking in seismic strength assessments of masonry buildings started with a fundamental paper of Housner [1963] in which he studied the rocking motion of a stone column resting on a rigid frictional base. We will reassume and comment the main results of Housner analysis.

A constant horizontal acceleration impulse of magnitude A_1 has been chosen here to represent schematically the perturbing action that hits the column at its initial vertical position: varying the duration t_1 of the impulse, this condition can give a simple qualitative representation of the seismic action (Figure 1, left).

Let us make reference to the Figure 1 (right) that shows the column in its rocking motion. The friction coefficient between the column and its basement is sufficiently large to prevent sliding. The column, at the position (1) (Figure 1, right), is falling down rotating around the base right corner O . When the column reaches the vertical position (2), its left base corner impacts against the basement rigid plane and an impulsive force suddenly takes place at the impact point O' and a change of motion suddenly occurs.



Figure 1. Constant horizontal acceleration impulse.

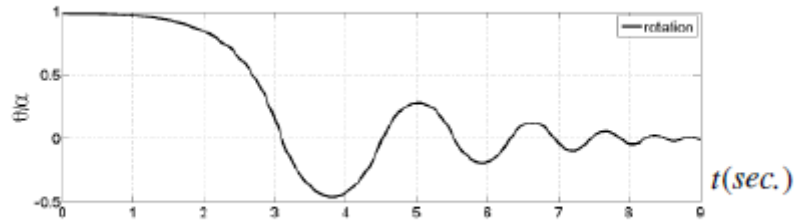


Figure 2. Damped oscillations of the column with gradually reducing amplitudes [Di Carlo 2014].

Just after the impact, the column begins to rotate now around the left base corner, the new point O' , the pivot of the new motion of the column. Dissipations of energy occur each time the column impacts on its base.

The column develops its swaying rocking motion oscillating around O and O' . Figure 2 shows this motion, with reducing amplitudes and shorter periods: it is of the inverted pendulum type, not harmonic but oscillatory, damped, in consequence of impacts. Rocking motion starts only if

$$A_1 \geq A_L = g \cdot t g \alpha, \quad (1)$$

where $t g \alpha = b/h$ defines the slenderness of the column having width b and height h .

Condition (1) shows that only if the magnitude A of the horizontal acceleration pulse A_1 is larger than $A_L = g \cdot t g \alpha$ — the magnitude of the acceleration that leads the pier to the limit equilibrium condition — the column puts itself in motion. At this point the resultant of all vertical and horizontal forces passes through the external edge O of the base section of the column, as shown in the left scheme of Figure 3.

The equation of the column motion hit by a constant horizontal acceleration impulse was firstly formulated in Housner [1963] as

$$I_0 \frac{d^2 \theta}{dt^2} = -W R (\alpha - \theta) + \frac{W A}{g} R. \quad (2)$$

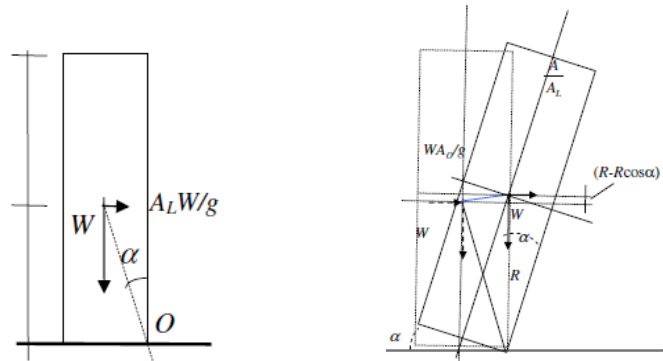


Figure 3. The solid column at the static failure and at the dynamical failure.

That, solved, gives

$$\theta(t) = \alpha \left(\frac{A}{A_L} - 1 \right) (\cosh pt - 1), \quad \frac{A}{A_L} > 1, \quad (3)$$

with

$$p = \sqrt{\frac{WR}{I_o}} = \sqrt{\frac{3g}{4h\sqrt{1+tg^2\alpha}}}. \quad (4)$$

The column, forced by an acceleration impulse A_0 , larger than A_L and of adequate duration t_0 , will continue to move sideways until to the inversion of the motion or, on the contrary, if the impulse acceleration and its duration are sufficiently high, until reaches the *critical* overturning configuration. This last state is defined by inclination (α) of the column at which any increment of the opposing action of the weight vanishes (Figure 3, right scheme).

The equation defining the intensity A_0 of this impulse, together with the corresponding duration t_0 , is obtained equating the work done by inertial force along the motion and during the whole time t_0 to the work required to raise the weight W of the column as far as to the limit position α :

$$\int_0^{t_1} \frac{W}{g} A_0 \frac{ds}{dt} dt = \frac{W}{g} A_0 R \int_0^{t_1} \dot{\theta}(t) dt = WR(1 - \cos \alpha). \quad (5)$$

Solution of condition (5) gives the relation occurring between the intensity A_0 of the acceleration impulse and its duration t_0 required to reach the critical dynamical overturning state [Housner 1963]

$$t_0 = \sqrt{\frac{4h\sqrt{1+tg^2\alpha}}{3g}} \cosh^{-1} \left(1 + \frac{1}{(2A_0/A_L)(A_0/A_L - 1)} \right). \quad (6)$$

A scale effect is present in (6) because two columns have the same ratio b/h , the higher requires a larger time duration t_0 to reach the failure under the same acceleration intensity A_0 . From the inspection of condition (6) we have

$$\frac{A_1}{A_L} \rightarrow \infty, \quad t_1 \rightarrow 0, \quad \frac{A_1}{A_L} \rightarrow 1, \quad t_1 \rightarrow \infty. \quad (7)$$

3. The masonry wall pier

3.1. Rocking with diagonal cracking. The wall pier is the vertical element of masonry walls with openings, the main resistant structural components of masonry buildings. Oblique cracking occurs in the masonry hit by horizontal actions and influence rocking.

On the wake of the above study of the Housner's solid column, let us examine the rocking motion of a wall pier (Figure 4, left) hit by a short horizontal acceleration pulse. Figure 4 (right) shows the wall pier at a generic cracked configuration, loaded by vertical forces — due to the self-weight of the element as to the weight of spandrels — and by the corresponding horizontal inertia forces.

The wall pier behaves quite differently from the solid column. This last can in fact only detach from its base while the masonry pier suffers from diagonal cracks.

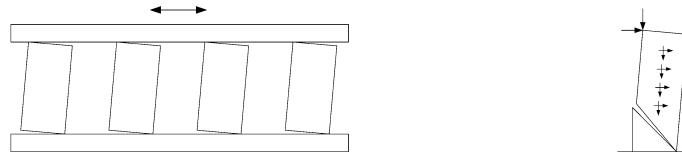


Figure 4. Generic configuration under alternate horizontal actions: masonry wall (left) and cracked wall pier (right).



Figure 5. The typical X-shaped cracking pattern occurring in a wall pier.

Rocking of the cracked pier, on the other hand, can effectively occur only if the inactive detached wedge of the block, represented by the dotted triangle in Figure 4 (right), does not crumble at the impacts with the pier tag-end, coming back during the inverted oscillation.

Answer to this question can be obtained by inspecting Figure 5 that shows the typical X-shaped cracking pattern occurred in a vertical pier, after the in-plane rocking of the wall. Analysis of the sequence of the cracking geometries occurring during the shaking movement that affects the scheme of a wall pier (see Figure 6) can better clarify the reasons of the development of these X-shaped cracks.

The first scheme (Figure 6) represents the undeformed configuration of the element. The second scheme shows the compressed right pier wedge, at the onset of the wall rotation. It moves along the first mechanism u^- in the clockwise direction and detaches from the left wedge, that remains ineffective. The third scheme shows the counter-clockwise rotation of the wedge that returns towards the vertical position still following the first mechanism u^- ; the fourth scheme refers to the contact occurring between the two wedges and to subsequent impact occurring at the left corner of the pier base. In the fifth scheme, the left wedge, following the subsequent returning mechanism u^+ , is detaching from the right one, thereby producing the other diagonal crack that, crossing with the first one, determines the detected X-shaped cracking, observed at the stop of the motion.

A prospective masonry destruction at the contact of the inactive wedge could not permit the occurrence of rocking. The presence of the X-shaped cracking, commonly detected in damaged walls of masonry buildings, proves that inactive masonry wedges are generally able to sustain, during the rocking, contacts with the other ones. At this contact the compression forces are, in fact, immediately conveyed as far as to the opposite corner of the pier base. Impact occurs just at this corner, the new pivot of the subsequent rotation mechanism u^+ . We remark that in both the Housner column and the masonry pier impact occurs at the hinge of the returning mechanism.

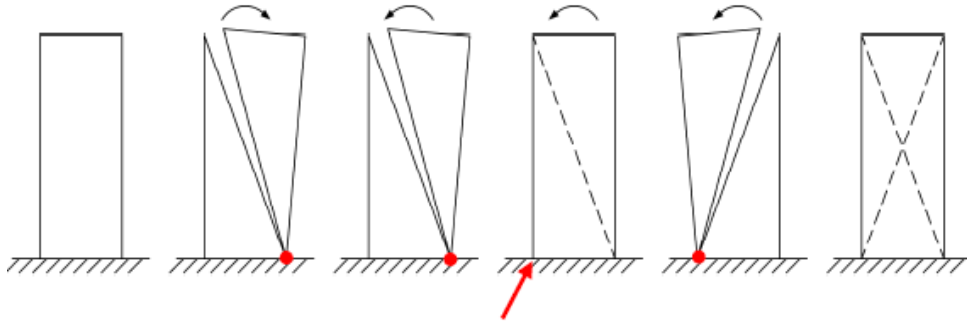


Figure 6. Sequence of the wall pier configurations during the formation of the X-shaped cracks.

3.2. Incipient rocking acceleration. As to the solid column, the rocking motion starts only if the magnitude A of the horizontal acceleration pulse is larger than A_L , the acceleration that leads the pier to the limit static equilibrium condition. At this state, in fact, the resultant of all vertical and horizontal forces passes exactly through the external edge O of the base section of the pier (Figure 7).

The value of the limit acceleration A_L equals the failure multiplier λ_0 of the horizontal inertia forces W/g , that can be obtained as application of the limit analysis approach.

As shown in Figure 7, a fracture KO , approximately assumed straight, starts at the section $K-K'$, at a distance ξ from the top of the element and reaches the toe O of the pier. This fracture splits the masonry block between the compressed portion and the ineffective one. The compressed region is composed by the upper uncracked rectangular parallelepiped of weight W_1 and by the lower triangular wedge of weight W_2 . The other triangular lower region located at the left side of the element is ineffective.

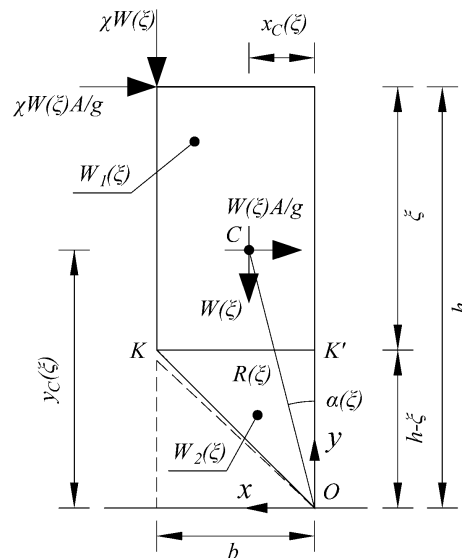


Figure 7. Forces acting during the rocking of the cracked wall pier.

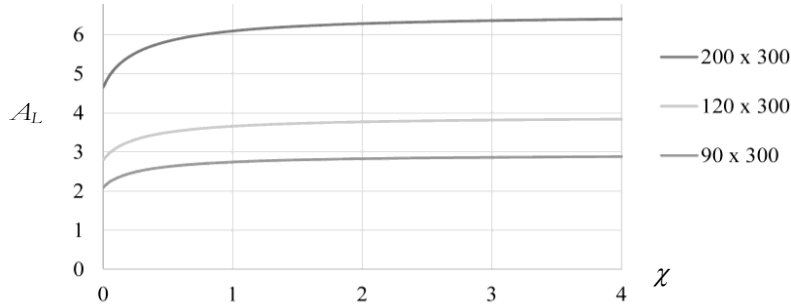


Figure 8. Incipient rocking acceleration A_L versus the factor χ varying the pier wall geometry.

A vertical force χW is applied at the head of the pier, being W the weight of the whole pier and χ a coefficient higher or equal to zero. The corresponding horizontal force is $\chi W A/g$, where A is the acceleration that hits the wall and g the gravity acceleration.

The magnitudes of the weights W_1 and W_2 depend on the distance ξ and, with reference to Figure 7, can be expressed as

$$W_1(\xi) = \gamma b \xi, \quad W_2(\xi) = \gamma \frac{b}{2} (h - \xi). \quad (8)$$

The weight W of all masses taking part in the mechanism is

$$W(\xi) = W_1(\xi) + W_2(\xi). \quad (9)$$

Defining the location of the gravity center C of all moving masses, the cracked configuration of the masonry pier at the incipient overturning is defined by the distance ξ and the limit acceleration A_L , which can be obtained by solving the following system of two equations:

$$\begin{aligned} W_1(\xi) \frac{A_L}{g} \frac{\xi}{2} + \chi W(\xi) \frac{A_L}{g} \xi &= W_1(\xi) \frac{b}{6} + \chi W(\xi) \frac{2}{3} b, \\ W_1(\xi) \frac{A_L}{g} \left(h - \frac{\xi}{2} \right) + W_2(\xi) \frac{A_L}{g} \frac{2}{3} (h - \xi) + \chi W(\xi) \frac{A_L}{g} h &= W_1(\xi) \frac{b}{2} + W_2(\xi) \frac{b}{3} + \chi W(\xi) b, \end{aligned} \quad (10)$$

respectively defining as the incipient cracking occurring at the section $K-K'$, as the incipient failure of the whole pier. The rocking of the pier, hit by a constant acceleration pulse of magnitude A , can actually start if $A > A_L$.

Figure 8 plots the incipient rocking acceleration A_L versus the ratio χ — i.e., the ratio between the load applied at the head and the whole weight of the pier — for the three considered geometries of the wall pier: a pier of 3 m height and a width variable between 0.9 m, 1.2 m and 2 m [Di Carlo et al. 2017].

3.3. Overturning caused by a constant acceleration pulse of finite duration. As in the Housner column, let us valuate the relation occurring at the dynamical collapse between the constant overturning acceleration A_0 and the corresponding critical duration t_0 .

The pier, hit by the horizontal acceleration pulse A , starts its motion in the cracked configuration, defined by the distance ξ : this last, together with the limit acceleration A_L , obtained by solving the system of (10).

Let I_0 be the moment of inertia around the point O of all the masses involved in the overturning of the pier. Making reference to the motion of the center C of all masses engaged, the equation of motion of the pier can be written as

$$I_0(\xi)\ddot{\theta} = -W(\xi)R(\xi)[\alpha(\xi) - \theta] + W(\xi)R(\xi)\frac{A}{g}, \quad (11)$$

that, with the position

$$p(\xi)^2 = \frac{W(\xi)R(\xi)}{I_0(\xi)},$$

has the solution

$$\theta(t) = [A/g - \alpha(\xi)][\cosh p(\xi)t - 1]. \quad (12)$$

The magnitude A_0 of an acceleration pulse having duration t_0 , required to overturn the block, is then given, likewise (5), by the condition

$$\frac{W(\xi)}{g}A_0 \int_0^{t_0} \frac{ds}{dt} dt = W(\xi)R(\xi)[1 - \cos \alpha(\xi)], \quad (13)$$

and we obtain

$$t_0 = \frac{1}{p(\xi)} \cosh^{-1} \left[1 + \frac{1}{\frac{2A_0}{A_L(\xi)} \left(\frac{A_0}{A_L(\xi)} - 1 \right)} \right], \quad (14)$$

that defines the dependence of the duration time t_0 from the impulse acceleration A_0 required to overturn the block. As it can be noted, equation (14) is characterized by the existence of vertical and horizontal asymptotes, being

$$\lim_{\frac{A_0}{A_L(\xi)} \rightarrow 1} t_0 = \infty, \quad \lim_{\frac{A_0}{A_L(\xi)} \rightarrow \infty} t_0 = 0. \quad (15)$$

With reference, for instance, to a 3 meters high and 0.9 meters wide pier, Figure 9 shows the trend of the overturning time t_0 varying the magnitude A_0 of the acceleration pulse, for different values of the coefficient χ varying in the range from 0 to 4 [Di Carlo et al. 2017]. The intercepts of the vertical asymptotes of the curves given by (14) with the horizontal axis give the corresponding magnitudes of the limit accelerations $A_L(\chi)$. The case $\chi = 0$ corresponds to the pier without masses applied at its top. This case is significant because is in direct correlation with the behavior of the Housner column.

Compared with the solid column, cracking occurring in the masonry pier implies either smaller duration t_0 of pulses with a given acceleration A_0 or, keeping fixed the duration t_0 , smaller magnitude of the overturning acceleration A_0 .

It is worth to note that the duration of the impulse required to overturn the pier wall increases with the increasing of the factor χ , i.e., of the magnitude of the mass applied at the pier top corner. It means that the presence of a mass applied at the pier head has thus a stabilizing effect, in spite of the corresponding increase in magnitude of the inertia horizontal force.

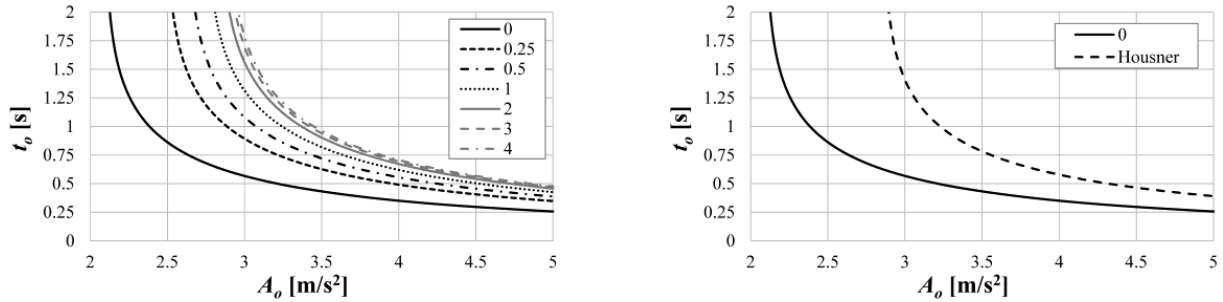


Figure 9. Plot of t_0 versus A_0 : varying the factor χ (left) and comparison with Housner's model (right).

4. Rocking of a masonry wall with opening and a steel tie

4.1. The limit static acceleration impulse. We will consider the scheme in Figure 10 as a simple wall composed by two masonry piers and a spandrel, connected by a top steel tie, in the oscillating motion activated by a sudden action of a constant horizontal impulse acceleration. It represents the simplest model of the multistorey walls with openings, composed by piers and spandrels, the main resistant structural components of the masonry building.

The acceleration impulse A induces on the wall a distribution of inertial horizontal loads. If the magnitude of the impulse is sufficiently high, the wall will reach the limit state and will deform according to the sideways swaying mechanism from the left to the right (Figure 11, left scheme). Cracking will occur at the bases of piers and the determination of the cracked layout of the piers, together with the limit horizontal acceleration A_L , can be achieved by the limit analysis approach [Di Carlo et al. ≥ 2019].

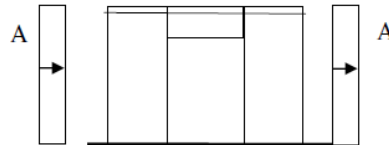


Figure 10

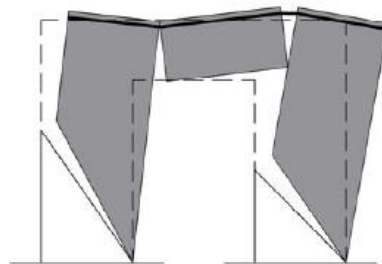


Figure 11. The rocking of the wall.

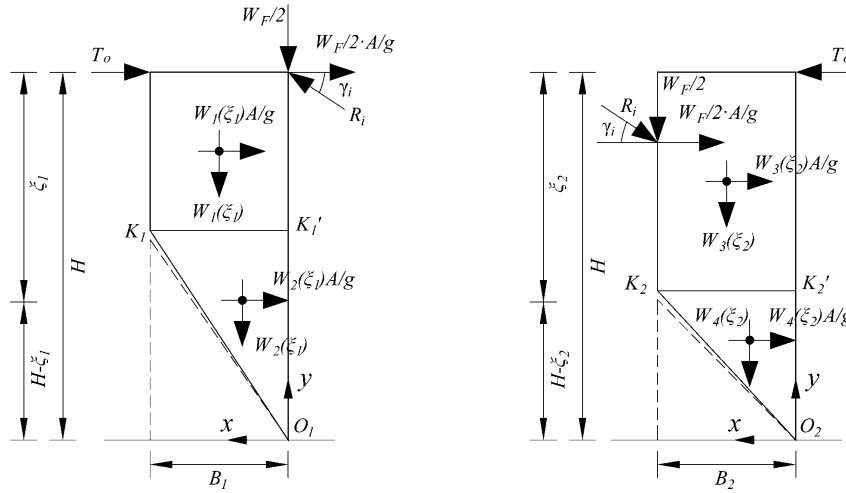


Figure 12. Forces on the cracked wall piers.

As shown in Figure 12, a fracture K_1C_1 (K_2C_2), assumed to be approximately straight, starts at the section $K_1-K'_1$ ($K_2-K'_2$), at a distance ξ_1 (ξ_2) from the top of the element and reaches the toe C_1 (C_2) of the pier. This fracture splits the masonry block into a compressed portion and in an ineffective part. The compressed region is composed by the upper uncracked rectangular parallelepiped of weight W_1 (W_3) and by the lower triangular wedge of weight W_2 (W_4). The other triangular lower region located at the left side of the element is ineffective. The semi-weights of the spandrel $W_F/2$ and the corresponding horizontal force $W_F/2 \cdot A/g$ are applied at hinges sections between piers and spandrel. The loading pattern on each of the piers is completed by the inclined compressive reaction R_i of the central panel. The magnitudes of the weights W_1 (W_3) and W_2 (W_4) depend on the distance ξ_1 (ξ_2) and, with reference to Figure 12, can be expressed as

$$W_1(\xi_1) = \gamma B_1 \xi_1, \quad W_2(\xi_1) = \gamma \frac{B_1}{2} (H - \xi_1), \quad (16)$$

and

$$W_3(\xi_2) = \gamma B_2 \xi_2, \quad W_4(\xi_2) = \gamma \frac{B_2}{2} (H - \xi_2). \quad (17)$$

The problem to define the cracked configuration of the masonry pier at the incipient overturning is a function of four unknowns: the two distances ξ_1 and ξ_2 , the reaction of the central panel R_i and the limit acceleration A_L . Two equations define the incipient cracking occurring at sections $K_1-K'_1$ and $K_2-K'_2$, respectively and another equation defines the limit equilibrium of the first pier.

For a given value of the limit acceleration A_L , let $\bar{\xi}_1$, $\bar{\xi}_2$ and \bar{R}_i be the solutions of these three equations that define the cracked zones of the piers and

$$W_1 = W_1(\bar{\xi}_1), \quad W_2 = W_2(\bar{\xi}_1), \quad W_3 = W_3(\bar{\xi}_2), \quad W_4 = W_4(\bar{\xi}_2), \quad (18)$$

are the weights of the four parts of the wall divided by cracks.

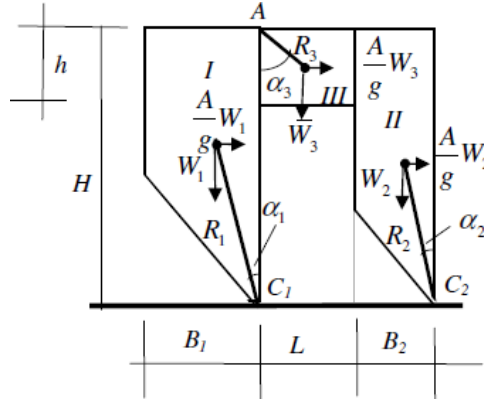


Figure 13. Geometry of the cracked swaying wall.

We can lump the weights W_1 and W_2 of the parts corresponding to the same pier at the corresponding centers G_1 and G_2 of the uncracked parts I and II. At the same time G_3 will represent the center of the spandrel where its weight W_3 is applied. At the cracked state, the essential wall geometry is described in Figure 13. Here the radii R_1 , R_2 and R_3 of vectors with their corresponding angles α_1 , α_2 and α_3 along the vertical axis can be easily determined.

The condition of the static global failure of the wall at the admissible cracking state is due to the action of a constant horizontal acceleration, acting so slowly on the wall to be represented by a static force. Thus applying the virtual work principle at limit equilibrium of the cracked state of the wall at the starting of the motion we get

$$\langle g, d\mathbf{u} \rangle + \delta L_{\text{tie}} + \langle \rho \mathbf{A}, d\mathbf{u} \rangle = 0, \quad t > 0, \quad (19)$$

where, with reference to the cracked configuration of the wall:

$$\langle g, \delta \mathbf{u} \rangle = - \sum_{i=1}^3 W_i R_i \sin \alpha_i d\theta_i, \quad (20)$$

is the resisting work of the dead loads g and $d\theta_1$, $d\theta_2$ and $d\theta_3$ are the small rotation increments of the three parts I, II, and III of the wall divided by cracks:

$$\delta L_{\text{tie}} = -T_0 H d\theta_1 (k_{21} - 1), \quad (21)$$

is the resisting plastic work in the steel tie:

$$\delta L_A = \frac{A_L}{g} \sum_{i=1}^3 W_i R_i d\theta_i \cos \alpha_i, \quad (22)$$

is the work of pushing inertial forces AW_i/g acting on the walls masses.

With the positions

$$\mu_{21} = \frac{W_2}{W_1}, \quad \mu_{31} = \frac{W_3}{W_1}, \quad \rho_{21} = \frac{R_2}{R_1}, \quad \rho_{31} = \frac{R_3}{R_1}, \quad (23)$$

we obtain the limit acceleration A_L :

$$A_L = g \frac{\sigma_{AL}}{\chi_{AL}}, \quad (24)$$

with

$$\sigma_{AL} = (\sin \alpha_1 + \mu_{21} \rho_{21} k_{21} \sin \alpha_2 + \mu_{31} \rho_{31} k_{31} \sin \alpha_3) + (T_0 H / W_1 R_1)(k_{21} - 1), \quad (25)$$

$$\chi_{AL} = (\cos \alpha_1 + \mu_{21} \rho_{21} k_{21} \cos \alpha_2 + \mu_{31} \rho_{31} k_{31} \cos \alpha_3). \quad (26)$$

It is worth to remark, on the other hand, that this result is valid if the stress state in the wall is statically admissible. To satisfy this condition, some local reinforcements can be placed at the top of piers in order to avoid local failures due to interactions between piers and spandrel.

4.2. Free rocking of the wall. Let us examine now the motion of the wall when, released at a sideways deformed configuration, it puts itself in motion going back to its initial position (Figure 14). In this stage, the motion is a fall and all the weights come down. The wall moves from the right to the left along the failure mechanism \mathbf{u}^- before it is determined by means of the limit analysis approach. This motion ends at the instant when simultaneous impacts occur between the piers with their basement as well as between piers and the central spandrel.

The second step goes from the instant of the inversion of motion, along the subsequent mechanism \mathbf{u}^+ , the *reverse* of the previous mechanism \mathbf{u}^- , i.e., having a mirrored hinges layout. Piers continue to rotate in clockwise direction while the spandrel, on the contrary, counter-clockwise. Impacts, between piers and the spandrel as well as between piers and the basement, take place at the positions of the new hinge of the mechanism \mathbf{u}^+ (Figure 14). Then the motion of the wall continues until the instant when the wall reaches the maximum side deformation, before to go back again and so on.

Let us consider the dynamical equilibrium of the wall in the first phase of this motion. Piers I and II are rotated of the angles θ_1 and θ_2 around their absolute centers C_1 and C_2 , while the central panel III is rotated of θ_3 around C_3 , all quantities connected by means of suitable kinematical conditions. This analysis is achieved by applying the principle of virtual displacements, evaluating, along a small deformation increment δu of the wall, the works done by the various engaged forces, *at the generic deformed configuration of the wall*, attained at the time t of the motion.

Application of the virtual work equation thus gives

$$\langle g, \delta \mathbf{u} \rangle + \delta L_{\text{tie}} - \langle \rho \ddot{\mathbf{u}}(t), \delta \mathbf{u} \rangle = 0, \quad t > 0, \quad (27)$$

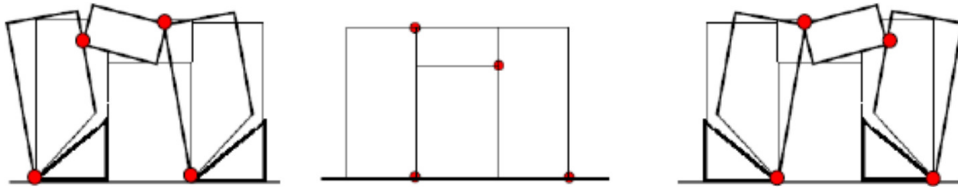


Figure 14. The motion of the wall at the instants just before and just after the impacts and the position of impact points.

where the work of the dead loads (g) is

$$\langle g, \delta u \rangle = \sum_{i=1}^3 W_i R_i \sin(\alpha_1 - \theta_1) d\theta_i, \quad (28)$$

and the work of the inertial loads is

$$-\langle \rho \ddot{u}(t), \delta u \rangle = \sum_{i=1}^3 I_{C_i}^{(i)} \ddot{\theta}_i d\theta_i, \quad (29)$$

with $I_{C_1}^{(1)}$, $I_{C_2}^{(2)}$, $I_{C_3}^{(3)}$ being the moments of inertia for the centers C_1 , C_2 , C_3 . The latter is the work of the stretch force T_0 in the steel tie. There is no release of energy in the steel tie with the assumed perfectly rigid plastic constitutive law (Figure 16) and $\delta L_{\text{tie}} = 0$. These works are all positive because all the weights W_1 , W_2 and W_3 move down as the wall falls along the mechanism with the outcome of the rotation increments $d\theta_1$, $d\theta_2$ and $d\theta_3$.

Continuing the analysis, whose development has been given in [Como 2016] we will reach the same conclusions about the features of the free rocking motion as in the case of the Housner solid column even if, in this case, the motion is influenced by cracking. These oscillations, that, due to the energy losses occurring at the impacts, become step by step faster and present gradually smaller amplitudes, are distinctive of the rocking motion.

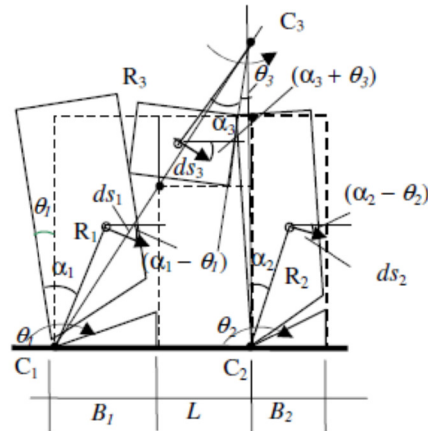


Figure 15. Geometry of the falling down mechanism of the first stage of motion.

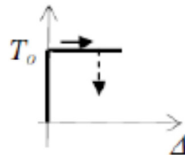


Figure 16. No release of energy in the steel tie at the unloading stage.

4.3. Impacts. As in the case of the column, the falling motion of the wall that moves along the mechanism (Figure 17, first scheme), stops at the instant $T/4$ when the wall reaches the undeformed “zero” configuration, a bit early than impacts will occur. At this instant all the hinges of the mechanism are closed and the motion cannot proceed along the same mechanism. At the “zero” configuration, contact will occur along the inclined fractures in the piers and along the connection sections piers/spandrel.

A compression flow thus immediately takes place along the ineffective masonry wedges and along the side sections of the spandrel. Inertial forces push the wall to continue its side motion, from the left to the right, so that it will activate a new mechanism with the formation of new hinges, placed in the “mirror” position with respect to the hinges of the previous mechanism.

At the reaching of the “zero” configuration, impacts will thus occur at the right corners of the base sections of the piers and at corners of the spandrel. In brief, impact points are thus spotted at the positions of the new mechanism (Figure 17). The velocities of the wall masses immediately before the impact — i.e., the rotational velocity $\dot{\theta}_1(T/4 - \varepsilon)$ of the pier I around C_1 and the velocities $\dot{\theta}_2$ and $\dot{\theta}_3$ — are known. Unknown, on the contrary, is the velocity $\dot{\theta}_{1p}(T/4 + \varepsilon)$ immediately after the impact. The knowledge of this velocity is on the other hand required to determine the second phase of the motion and the energy loss due to the impact. The determination of this velocity can be performed by applying the principles of impulse and angular momentum.

This application involves other unknown quantities, i.e., the impulses $F_1 dt$, $F_2 dt$, acting at the impact points between the piers I and II and their base sections. It is thus necessary to consider suitable applications in sequence of the above principles. First, from the principle of the impulse applied to the whole system of Figure 18, immediately before and immediately after the impact, in the coordinate directions x and y , we have

$$mv_x(T/4 - \varepsilon) + IMP_x = mv_x(T/4 + \varepsilon), \quad (30)$$

$$mv_y(T/4 - \varepsilon) + IMP_y = mv_y(T/4 + \varepsilon). \quad (31)$$

Likewise, from the principle of the angular momentum applied to the whole system around the impact point A of the first pier with the basement (Figure 18), we have

$$\Lambda_A(T/4 - \varepsilon) + \mathcal{M}_A dt = \Lambda_A(T/4 + \varepsilon). \quad (32)$$

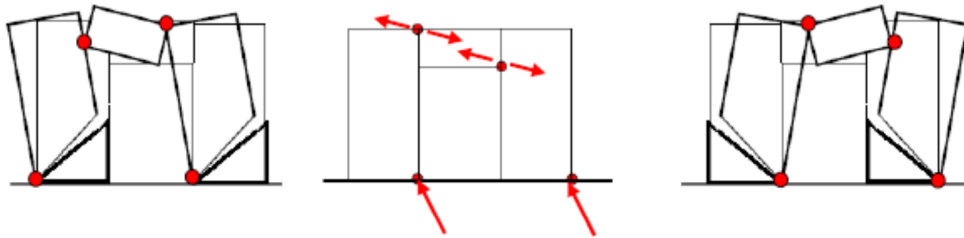


Figure 17. wall configuration just before impacts, impacts, wall configuration subsequent impacts.

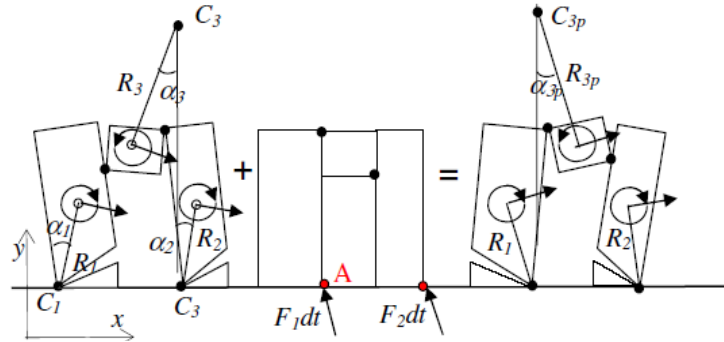


Figure 18. Application of the impulse principle to the whole system.

Similarly, applying to the first pier the principle of the angular momentum around the impact point B with the central panel (Figure 19, left), we have

$$\Lambda_B^{(1)}(T/4 - \varepsilon) + \mathcal{M}_B^{(1)} dt = \Lambda_B^{(1)}(T/4 + \varepsilon). \quad (33)$$

Finally, applying to the second pier the principle of the angular momentum around the impact point C with the central panel (Figure 19, right), we have

$$\Lambda_C^{(2)}(T/4 - \varepsilon) + \mathcal{M}_C^{(2)} dt = \Lambda_C^{(2)}(T/4 + \varepsilon). \quad (34)$$

Taking into account that

$$\dot{\theta}_2 = k_{21} \dot{\theta}_1, \quad \dot{\theta}_3 = k_{31} \dot{\theta}_1, \quad \dot{\theta}_{2p} = k_{21p} \dot{\theta}_{1p}, \quad \dot{\theta}_{3p} = k_{31p} \dot{\theta}_{1p}, \quad (35)$$

with the suitable connection factors k_{21} , k_{31} , k_{21p} and k_{31p} , the five equations (30), (31), (32), (33) and (34) can be solved, determining the five unknowns F_{1x} , F_{1y} , F_{2x} , F_{2y} and $\dot{\theta}_{1p}(T/4 + \varepsilon)$. A numerical application has been performed considering a simple masonry wall composed by 2 m wide piers and one spandrel, having a length of 2 m and a height of 1.2 m.

Two values of the height of the piers have been considered, 4 m and 6 m, respectively. The ratio between the rotational velocities immediately after and immediately before the impact results to be 0.181 and 0.413, respectively.

As in the Housner column [Housner 1963], the coefficient of restitution increases with the increasing of the slenderness of the system.

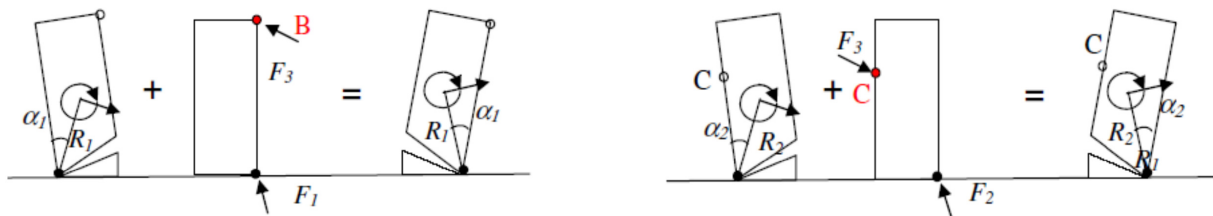


Figure 19. The principle of angular momentum: on the first pier around the impact point B (left) and on the second pier around the impact point C (right).

4.4. Forced motion of the wall hit by an acceleration impulse of given duration. Let us consider now a generic deformed configuration of the wall while it is pushed by a constant horizontal acceleration impulse A of given duration t . The corresponding motion of the wall is achieved as an application of the principle of virtual displacements, evaluating, along a small deformation increment δu , the works done by the various engaged forces, *at the generic deformed configuration of the wall*—defined by the rotation angles $\theta_1, \theta_2, \theta_3$, occurring around the absolute centers of the three panels in which the wall is subdivided—attained at time t of the motion (Figure 20). We get

$$\langle \mathbf{g}, \delta \mathbf{u} \rangle + \delta L_{\text{tie}} - \langle \rho \ddot{\mathbf{u}}(t) + \rho \mathbf{A}, \delta \mathbf{u} \rangle = 0, \quad t > 0, \quad (36)$$

where the work of the dead loads is

$$\langle \mathbf{g}, \delta \mathbf{u} \rangle = -W_1 ds_1 \sin(\alpha_1 - \theta_1) - W_2 ds_2 \sin(\alpha_2 - \theta_2) - W_3 ds_3 \sin(\alpha_3 + \theta_3), \quad (37)$$

where, with reference to Figure 20 $ds_1 = R_1 d\theta_1$, $ds_2 = R_2 d\theta_2$, $ds_3 = R_3 d\theta_3$ and

$$\langle \mathbf{g}, \delta \mathbf{u} \rangle = -W_1 R_1 d\theta_1 \sin(\alpha_1 - \theta) - W_2 R_2 d\theta_2 \sin(\alpha_2 - \theta_2) - W_3 R_3 d\theta_3 \sin(\alpha_3 + \theta_3). \quad (36')$$

During the increasing wall sideways displacement, the steel tie stretches at the yielding state. We have

$$\delta L_{pl} = -T_0(k_{21} - 1)H \delta\theta_1. \quad (38)$$

Summing up all the works, with the positions

$$\lambda_A = (\cos \alpha_1 + \mu_{21}\rho_{21}k_{21} \cos \alpha_2 + \mu_{31}\rho_{31}k_{31} \cos \alpha_3) = \chi_{AL}, \quad (39)$$

$$\sigma_A = \sin \alpha_1 + \mu_{21}\rho_{21}k_{21}^2 \sin \alpha_2 - \mu_{31}\rho_{31}k_{31}^2 \sin \alpha_3, \quad (40)$$

$$\sigma_{A\text{asc}} = \sin \alpha_1 + \mu_{21}\rho_{21}k_{21} \sin \alpha_2 + \mu_{31}\rho_{31}k_{31} \sin \alpha_3 + T_0 H(k_{21} - 1)/W_1 R_1 = \sigma_{AL}, \quad (41)$$

$$\chi_{A\text{asc}} = (\cos \alpha_1 + \mu_{21}\rho_{21}k_{21}^2 \cos \alpha_2 - \mu_{31}\rho_{31}k_{31}^2 \cos \alpha_3), \quad (42)$$

$$p_*^2 = \frac{W_1 R_1}{I_C^*} \chi_{A\text{asc}}, \quad (43)$$

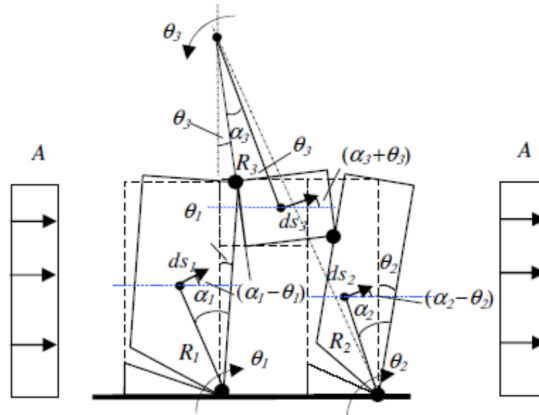


Figure 20. The wall in an ascending motion dragged by the horizontal acceleration impulse A .

the equation of the forced motion of the wall simplifies and becomes

$$\ddot{\theta}_1 - p_*^2 \theta_1 = -\frac{p_*^2}{\chi_{Aasc}} \left(\sigma_{AL} - \frac{A}{g} \chi_{AL} \right), \quad (44)$$

whose solution, satisfying the initial conditions $\theta_1(0) = \dot{\theta}_1(0) = 0$, is

$$\theta_1(t) = \Phi(\cosh p_* t - 1), \quad (45)$$

where

$$\Phi = \frac{1}{\chi_{Aasc}} \left(\frac{A}{g} \chi_{AL} - \sigma_{AL} \right). \quad (46)$$

4.5. Dynamical collapse. There is a configuration C_0 of the wall along the side motion $\theta = \theta_1(t)$ at which the potential energy of all the weights acting on the wall reaches its maximum. When the wall reaches this configuration, weights no longer oppose any displacement increment starting from C_0 . The dynamical collapse of the wall is thus attained if the acceleration impulse has sufficient intensity A_1 and sufficient duration t_0 so that the inertial forces, induced by A_1 , move, just in the time t_0 , the wall along motion $\theta = \theta_1(t)$ as far as the configuration C_0 has been reached. Hence, taking into account that

$$\dot{\theta}_1(t) = \Phi p_* \sinh p_* t, \quad \dot{\theta}_2(t) = k_{21} \dot{\theta}_1(t), \quad \dot{\theta}_3(t) = k_{31} \dot{\theta}_1(t), \quad (47)$$

and with reference, for the sake of simplicity, to Figure 21, that shows the raising of the weight W_1 , we get that the difference in potential energy between the deformed and the initial configurations of the wall, can be evaluated as

$$\Delta E = \sum_{i=1}^3 W_i R_i [\cos(\alpha_i - \theta_i) - \cos \alpha_i]. \quad (48)$$

At the same time the work done along the motion by the horizontal push due to the acceleration impulse, making reference to Figure 20, is

$$L_{IMP} = \frac{A_0}{g} \sum_{i=1}^3 W_i R_i \int_0^{t_0} \frac{ds_i}{dt} \cos(\alpha_i - \theta_i) dt. \quad (49)$$

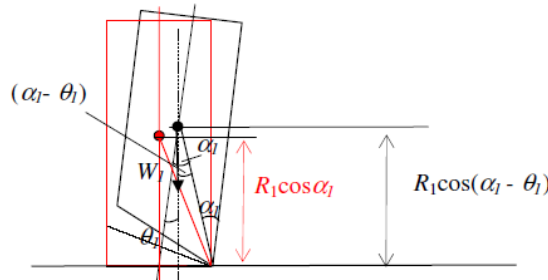


Figure 21. The raising of the weight W_1 of the pier I.

Finally, the balance between the work of the inertial forces and the potential energy increment, gives

$$L_{IMP} = \frac{A_0}{g} \sum_{i=1}^3 W_i R_i \int_0^{t_0} \frac{ds_i}{dt} \cos(\alpha_i - \theta_i) dt = \Delta E = \sum_{i=1}^3 W_i R_i [\cos(\alpha_i - \theta_i) - \cos \alpha_i]. \quad (50)$$

Evaluating the integrals up to the time t_0 , the dynamical failure condition is

$$\begin{aligned} L_{IMP} &= \Phi \frac{A_0}{g} \frac{1}{p_*} \left(\{w_1 R_1 \cos \alpha_1 + w_2 R_2 k_{21} \cos \alpha_2 + w_3 R_3 k_{31} \cos \alpha_3\} (\cosh p_* t_0 - 1) \right. \\ &\quad \left. + \{w_1 R_1 \sin \alpha_1 + w_2 R_2 k_{21}^2 \sin \alpha_2 - w_3 R_3 k_{31}^2 \sin \alpha_3\} \left[\frac{\sinh^2 p_* t_0}{2} - \cosh p_* t_0 + 1 \right] \right) \\ &= MAX W_1 R_1 [\cos(\alpha_1 - \theta_1) - \cos \alpha_1] + W_2 R_2 [\cos(\alpha_2 - \theta_2) - \cos \alpha_2] \\ &\quad + W_3 R_3 [\cos \alpha_3 - \cos(\alpha_3 + \theta_3)], \end{aligned} \quad (51)$$

correlating the magnitude of the acceleration impulse A_0 with its duration t_0 .

We point out that when $t_0 \rightarrow \infty$, $\Phi \rightarrow 0$. In this case the value of the acceleration impulse A_0 coincides with the value of the acceleration impulse A_L , determining the static failure of the wall. We have in fact, with (51)

$$\Phi \rightarrow 0 \Leftrightarrow \frac{1}{\chi_{Aasc}} \left(\frac{A}{g} \chi_{AL} - \sigma_{AL} \right) \rightarrow 0 \Leftrightarrow \frac{A}{g} \chi_{AL} \rightarrow \sigma_{AL} \Leftrightarrow \frac{A}{g} \rightarrow \frac{\sigma_{AL}}{\chi_{AL}} = A_L, \quad (52)$$

matching (24). A numerical investigation is carried out in order to clarify the described procedure and to practically show how to evaluate the incipient rocking and collapse accelerations. For the sake of simplicity, a simple geometry of the wall, characterized by two piers and one storey, is considered in the following.

The side view of the active wall is shown in Figure 22 (left), together with the indication of the main geometrical parameters. Both piers and the spandrel have the same thickness. In particular, the widths of the two piers are equal to 2 m and 2.5 m, while their height is equal to 6 m. The spandrel is 2 m wide and 1.5 m high.

The specific weight of the masonry material is taken to be equal to 16 kN/m^3 . The incipient rocking acceleration value A_L is evaluated and it is equal to 3 m/s^2 . The cracked configuration is defined by the distances ξ_1 and ξ_2 of the sections in which the cracks start from the top of the piers, equal to 2.73 m and 3.47 m, respectively. The fourth unknown is the diagonal reaction of the spandrel, equal to 16.8 kN.

The dynamical failure condition of the wall, pushed by a constant horizontal acceleration impulse of given duration, is obtained by solving (51). By varying the duration t_0 of the impulse, it is thus possible to evaluate the magnitude of the collapse acceleration A_0 .

In this way, we can define a failure domain of the masonry wall, numerically solving (51), finding different combinations of values of pulse magnitude and duration, which lead the system to the achievement of a failure condition. Figure 22 (right) shows the failure domain of the considered scheme of masonry wall, in terms of the ratio between collapse and activation accelerations. The domain located below the curve corresponds to an equilibrium condition, while the upper part of the graph refers to the attainment of a failure state.

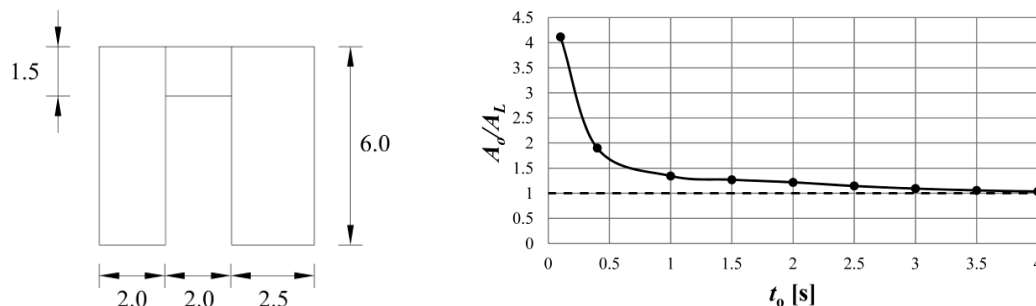


Figure 22. Left: geometry of the masonry wall. Right: failure domain of the examined masonry wall.

The horizontal dashed line (Figure 22, right) indicates the load multiplier value required for the activation of the motion, evaluated through the equivalent static analysis: it represents a horizontal asymptote of the failure domain, attainable for infinite values of the pulse duration. The zone of the graph located under this value represents a rest condition of the system. Figure 22 (right) shows the trend of the ratio A_0/A_L between the dynamical constant acceleration impulse A_0 and the static limit acceleration A_L versus its duration time t_0 . It is recognized from this graph that for a duration time $t_0 = 0.25$ s—a value corresponding to a strong seismic shock—the ratio $A_0/A_L = 2.5$. It means that in this case the intensity of the acceleration impulse determining the dynamic failure of the wall is 2.5 times larger than the static limit acceleration usually considered to evaluate the seismic strength of the wall.

If we consider the peak ground acceleration a_{PGa} representative of the seismic shock of the given site, equating A_0 to a_{PGa} , we can assume static limit acceleration A_L 2.5 lower than a_{PGa} . The ratio $A_0(t_0)/A_L$ can thus be considered as the reduction factor q to assume checking the seismic strength of the wall, rather than values obtained by assumptions founded on a doubtful masonry ductility.

5. Conclusions

The paper has examined the rocking of some important structural schemes by using an analytical approach, starting from the solid column to the masonry pier, and then to a simple model of a masonry wall, composed by two piers and a spandrel, connected by a steel chain. The dynamic action applied to these models is a horizontal acceleration impulse at given intensity and duration.

The rocking capacity of these models has been thoroughly examined under these dynamic loadings, firstly to obtain useful information concerning the maximum acceleration intensity, corresponding to a given duration, able to produce the dynamic failure of the structure. Impacts occurring during the rocking motion have been analyzed to determine the corresponding dynamical energy losses able to give information on the dissipation of energy occurring during the motion, dissipation at a first sight unexpected in masonry structures that, deform with mechanisms with hinges that open without any material opposition.

The intensity of the dynamic acceleration impulse able to produce the dynamical collapse can be much larger than the limit static acceleration; this last is the representative of the seismic side strength of the structure.

These results, in some points innovative, recall some issues of the author and others [Coccia et al. 2016; Di Carlo et al. 2017] and point out the usefulness of dynamical approaches to obtain sound evaluations of the strength reduction factor q , fundamental in checking the seismic strength of constructions.

References

- [Coccia et al. 2016] S. Coccia, F. Di Carlo, and S. Imperatore, “Force reduction factor for out-of-plane simple mechanisms of masonry structures”, *Bull. Earthq. Eng.* **15**:3 (2016), 1241–1259.
- [Como 2016] M. Como, *Statics of historic masonry constructions*, 2nd ed., Springer, Switzerland, 2016.
- [Di Carlo 2014] F. Di Carlo, *Strength reduction factor, for rocking masonry structures*, Ph.D. dissertation, Department of Civil Engineering and Computer Science Engineering, University of Rome Tor Vergata, 2014.
- [Di Carlo et al. 2017] F. Di Carlo, S. Coccia, and M. Como, “Rocking in presence of cracking of masonry wall piers”, *Key Eng. Mater.* **747** (2017), 678–685.
- [Di Carlo et al. \geq 2019] F. Di Carlo, S. Coccia, and M. Como, “Rocking of cracked masonry walls loaded by constant impulse acceleration”, to appear in *Meccanica (Milano)*.
- [Giannini and Masiani 1996] R. Giannini and R. Masiani, “Non-Gaussian solution for random rocking of slender rigid block”, *Probab. Eng. Mech.* **11**:2 (1996), 87–96.
- [Heyman 1992] J. Heyman, “Leaning towers”, *Meccanica (Milano)* **27**:3 (1992), 153–159.
- [Hogan 1992] S. J. Hogan, “On the motion of a rigid block, tethered at one corner, under harmonic forcing”, *Proc. R. Soc. Lond. A* **439**:1905 (1992), 35–45.
- [Housner 1963] G. W. Housner, “The behaviour of inverted pendulum structures during earthquakes”, *Bull. Seismol. Soc. Am.* **53**:2 (1963), 403–417.
- [Liberatore et al. 2002] D. Liberatore, G. Spera, G. D’Alessandro, and D. Nigro, “Rocking of slender blocks subjected to seismic motion of the base”, in *Twelfth European Conference on Earthquake Engineering* (London), 2002.
- [Ochserdorf 2002] J. A. Ochserdorf, *Collapse of masonry structures*, Doctoral thesis, Department of Engineering, University of Cambridge, 2002, Available at <https://www.repository.cam.ac.uk/handle/1810/244820>.
- [Peña et al. 2007] F. Peña, F. Prieto, P. B. Lourenço, A. Campos Costa, and J. V. Lemos, “On the dynamics of rocking motion of single rigid-block structures”, *Earthq. Eng. Struct. Dyn.* **36**:15 (2007), 2383–2399.
- [Sorrentino et al. 2006] L. Sorrentino, R. Masiani, and L. D. Decanini, “Overturning of rocking rigid bodies under transient ground motions”, *Struct. Eng. Mech.* **22**:3 (2006), 293–310.
- [Sorrentino et al. 2008] L. Sorrentino, R. Masiani, and M. C. Griffith, “The vertical spanning strip wall as a coupled rocking rigid body assembly”, *Struct. Eng. Mech.* **29**:4 (2008), 433–453.
- [Yim et al. 1980] C.-S. Yim, A. K. Chopra, and J. Penzien, “Rocking response of rigid blocks to earthquakes”, *Earthq. Eng. Struct. Dyn.* **8**:6 (1980), 565–587.

Received 27 May 2018. Revised 27 Sep 2019. Accepted 18 Oct 2019.

MARIO COMO: como@ing.uniroma2.it

Department of Civil Engineering and Computer Science Engineering (DICII), University of Rome Tor Vergata,
Via del Politecnico 1, 00133 Rome, Italy

JOURNAL OF MECHANICS OF MATERIALS AND STRUCTURES

msp.org/jomms

Founded by Charles R. Steele and Marie-Louise Steele

EDITORIAL BOARD

ADAIR R. AGUIAR	University of São Paulo at São Carlos, Brazil
KATIA BERTOLDI	Harvard University, USA
DAVIDE BIGONI	University of Trento, Italy
MAENGHYO CHO	Seoul National University, Korea
HUILING DUAN	Beijing University
YIBIN FU	Keele University, UK
IWONA JASIUK	University of Illinois at Urbana-Champaign, USA
DENNIS KOCHMANN	ETH Zurich
MITSUTOSHI KURODA	Yamagata University, Japan
CHEE W. LIM	City University of Hong Kong
ZISHUN LIU	Xi'an Jiaotong University, China
THOMAS J. PENCE	Michigan State University, USA
GIANNI ROYER-CARFAGNI	Università degli studi di Parma, Italy
DAVID STEIGMANN	University of California at Berkeley, USA
PAUL STEINMANN	Friedrich-Alexander-Universität Erlangen-Nürnberg, Germany
KENJIRO TERADA	Tohoku University, Japan

ADVISORY BOARD

J. P. CARTER	University of Sydney, Australia
D. H. HODGES	Georgia Institute of Technology, USA
J. HUTCHINSON	Harvard University, USA
D. PAMPLONA	Universidade Católica do Rio de Janeiro, Brazil
M. B. RUBIN	Technion, Haifa, Israel

PRODUCTION production@msp.org

SILVIO LEVY Scientific Editor

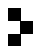
Cover photo: Mando Gomez, www.mandolux.com

See msp.org/jomms for submission guidelines.

JoMMS (ISSN 1559-3959) at Mathematical Sciences Publishers, 798 Evans Hall #6840, c/o University of California, Berkeley, CA 94720-3840, is published in 10 issues a year. The subscription price for 2019 is US \$635/year for the electronic version, and \$795/year (+\$60, if shipping outside the US) for print and electronic. Subscriptions, requests for back issues, and changes of address should be sent to MSP.

JoMMS peer-review and production is managed by EditFlow® from Mathematical Sciences Publishers.

PUBLISHED BY

 **mathematical sciences publishers**
nonprofit scientific publishing

<http://msp.org/>

© 2019 Mathematical Sciences Publishers

Journal of Mechanics of Materials and Structures

Volume 14, No. 5

December 2019

Preface	MAURIZIO ANGELILLO and SANTIAGO HUERTA FERNÁNDEZ	601
Studying the dome of Pisa cathedral via a modern reinterpretation of Durand-Claye's method	DANILO AITA, RICCARDO BARSOTTI and STEFANO BENNATI	603
Experimental and numerical study of the dynamic behaviour of masonry circular arches with non-negligible tensile capacity	ALEJANDRA ALBUERNE, ATHANASIOS PAPPAS, MARTIN WILLIAMS and DINA D'AYALA	621
Influence of geometry on seismic capacity of circular buttressed arches	GIUSEPPE BRANDONISIO and ANTONELLO DE LUCA	645
Failure pattern prediction in masonry	GIANMARCO DE FELICE and MARIALAURA MALENA	663
Energy based fracture identification in masonry structures: the case study of the church of "Pietà dei Turchini"	ANTONINO IANNUZZO	683
Displacement capacity of masonry structures under horizontal actions via PRD method	ANTONINO IANNUZZO, CARLO OLIVIERI and ANTONIO FORTUNATO	703
Automatic generation of statically admissible stress fields in masonry vaults	ELENA DE CHIARA, CLAUDIA CENNAMO, ANTONIO GESUALDO, ANDREA MONTANINO, CARLO OLIVIERI and ANTONIO FORTUNATO	719
Limit analysis of cloister vaults: the case study of Palazzo Caracciolo di Avellino	ANTONIO GESUALDO, GIUSEPPE BRANDONISIO, ANTONELLO DE LUCA, ANTONINO IANNUZZO, ANDREA MONTANINO and CARLO OLIVIERI	739
The rocking: a resource for the side strength of masonry structures	MARIO COMO	751



1559-3959(2019)14:5;1-T